J. Innovative Eng. Nat. Sci., vol. 5, no. 2, pp. 824-837, 2025.
http://doi.org/10.61112/jiens.1731536

JIENS
Journal of Innovative Engineering and Natural Science
(Yenilikçi Mühendislik ve Doğa Bilimleri Dergisi)
https://dergipark.org.tr/en/pub/jiens
Original Paper

Effect of microwave-reduced graphene oxide on the mechanical, thermal, and physical properties of banana fiber reinforced epoxy composites

Yasin Altin[a,b,*]

[a]Department of Polymer Materials Engineering, Bursa Technical University, Bursa 16310, Türkiye.
[b]Central Research Laboratory, Bursa Technical University, Bursa 16310, Türkiye.

ARTICLE INFO

Article history:
Received 2 May 2025
Received in revised form 1 July 2025
Accepted 21 July 2025

Available online

Keywords:
Banana fiber
Epoxy composites
Reduced graphene oxide
Microwave reduction
Mechanical properties
Natural fiber reinforcement

ABSTRACT

This study presents a comprehensive investigation into enhancing the mechanical and thermal performance of banana fiber-reinforced epoxy composites through the incorporation of microwave-reduced graphene oxide (rGO) as a nanofiller. Graphene oxide (GO) was synthesized from graphite powder via the improved Hummers' method. Its successful synthesis and subsequent reduction to rGO were confirmed by Fourier-transform infrared (FT-IR) and Raman spectroscopy. Raman analysis revealed a characteristic increase in the defect ratio (I_D/I_G) from 0.12 for pristine graphite to 0.896 for GO, and further to 0.963 for rGO. This trend indicates the formation of numerous, smaller sp^2 domains upon reduction, a key factor for effective reinforcement. Composite laminates were fabricated by hand lay-up with rGO loadings of 0, 0.1, 0.2, and 0.5 wt.%. Mechanical and thermal properties were analyzed. The results demonstrated that the effect of rGO is highly dependent on concentration. For tensile properties, the optimal performance was achieved at 0.2 wt.% rGO, while flexural properties were maximized at 0.5 wt.%. Physical property analysis revealed a decrease in composite density with increasing reinforcement content, a trend attributed to the inherent porosity (lumen) of the banana fibers themselves. Optical microscopy images confirmed the homogeneous distribution of fibers in the matrix, a key factor for composite performance. This research highlights the complex role of rGO in natural fiber composites and underscores the importance of optimizing filler content for specific application requirements.

I. INTRODUCTION

The global push towards a sustainable and circular economy has intensified the search for advanced materials that are not only high-performing but also environmentally benign. Polymer matrix composites (PMCs) have become indispensable in high-tech sectors such as aerospace, automotive, and marine industries due to their exceptional specific strength, stiffness, and corrosion resistance [1, 2]. Traditionally, these composites have been reinforced with synthetic fibers like carbon and glass. However, the significant energy consumption, high cost, non-biodegradability, and reliance on fossil fuels associated with these fibers have created a pressing need for sustainable alternatives [3, 4].

In this context, natural lignocellulosic fibers derived from plants such as jute, kenaf, sisal, and banana have garnered substantial attention as viable reinforcements for polymers [5, 6]. These fibers present a compelling suite of advantages: they are renewable, biodegradable, abundant, low-cost, and possess low density coupled with high specific mechanical properties [7, 8]. Among these, banana fiber, an agricultural by-product of banana cultivation, is particularly promising due to its high cellulose content (63–64%), significant tensile strength, and low elongation at break, making it a strong candidate for reinforcing polymer composites [9, 10].

*Corresponding author. Tel.: +90-224-808-1121; e-mail: yasin.altin@btu.edu.tr

Despite their potential, the effective utilization of natural fibers in PMCs is hindered by a fundamental challenge: the poor interfacial adhesion between the hydrophilic, polar nature of the lignocellulosic fibers and the hydrophobic, non-polar character of most polymer matrices, including epoxy [11]. Epoxy resins are widely utilized in composite science due to their excellent mechanical properties, chemical resistance, and strong adhesion to various substrates, making them suitable for both high-performance structural composites [1, 8] and advanced adhesive formulations [12]. However, the surface of natural fibers is rich in hydroxyl (-OH) groups, which attract water molecules but repel non-polar polymer chains. This incompatibility leads to a weak fiber-matrix interface, characterized by voids and micro-gaps, which impedes efficient stress transfer from the matrix to the load-bearing fibers. Consequently, this weak interface often becomes the point of premature failure, preventing the composite from reaching its full mechanical potential [13, 14]. To mitigate this issue, various strategies such as fiber surface modifications (e.g., alkali treatment, plasma treatment) and the incorporation of compatibilizers or nanofillers have been extensively explored [15].

The advent of nanotechnology has opened new avenues for enhancing the interfacial properties of composites. Graphene, a two-dimensional monolayer of sp^2-hybridized carbon atoms, and its derivatives have emerged as revolutionary nanofillers due to their extraordinary properties: a Young's modulus of approximately 1 TPa, intrinsic strength of 130 GPa, and a theoretical specific surface area of ~2630 m^2/g [16, 17]. Graphene oxide (GO), a functionalized form of graphene, is particularly well-suited for this application. The presence of oxygen-containing functional groups (hydroxyl, epoxy, carboxyl) on its basal planes and edges makes it readily dispersible in polar matrices like epoxy and allows it to form strong hydrogen or covalent bonds with the hydroxyl groups on the surface of natural fibers [18, 19].

While GO enhances dispersion and interfacial bonding, its disrupted sp^2 carbon lattice compromises the mechanical and electrical properties of pristine graphene. A subsequent reduction step to produce reduced graphene oxide (rGO) is therefore essential. This process removes a significant portion of the oxygen groups, largely restoring the conjugated sp^2 network and, with it, the exceptional properties of graphene [20]. Among various reduction techniques, microwave-assisted reduction has proven to be a particularly attractive method. It is a rapid, solvent-free, and energy-efficient process that leverages the dielectric properties of GO to induce a "thermal shock," causing simultaneous exfoliation and reduction in a matter of minutes [21, 22]. The resulting rGO possesses a high surface area and a wrinkled morphology, which is ideal for promoting mechanical interlocking within the polymer matrix.

Therefore, this study aims to synthesize rGO via a microwave-assisted route and investigate its effect as a nanofiller on the mechanical and interfacial properties of alkali-treated banana fiber-reinforced epoxy composites. By systematically varying the weight percentage of rGO (0%, 0.1%, 0.2%, and 0.5%), we seek to: (i) evaluate the impact of rGO on the tensile, compressive, and flexural properties of the composites; (ii) identify the optimal rGO concentration that maximizes mechanical performance; and (iii) elucidate the underlying strengthening mechanisms by conducting a thorough microstructural analysis of the fracture surfaces. This research aims to contribute to the development of a new class of lightweight, high-strength, and sustainable bio-composites for advanced structural applications.

II. EXPERIMENTAL METHOD

2.1 Materials

Epoxy (LR285) and hardener (H287) was obtained from Kompozitnet (İstanbul-TURKEY). Reinforcement fibers were obtained from local supplier. For nanofiller synthesis, graphite powder, sulfuric acid (H_2SO_4, 98%), phosphoric acid (H_3PO_4, 85%), potassium permanganate ($KMnO_4$), hydrogen peroxide (H_2O_2, 30%), and hydrochloric acid (HCl, 37%) were purchased from Sigma-Aldrich. All chemicals and reagents were used as received without further purifications.

2.2 Surface Treatment of Banana Fiber

To enhance fiber-matrix adhesion, the raw banana fibers were subjected to an alkali treatment. Following the procedure outlined by Özen et al. [15] for jute fibers, the banana fibers were immersed in a 1M NaOH solution at 90 °C for 1 hour. This treatment effectively removes impurities like hemicellulose, lignin, and waxes, and increases the surface roughness, thereby promoting better mechanical interlocking with the epoxy matrix. Post-treatment, the fibers were washed with distilled water until a neutral pH was reached and subsequently dried in an oven at 80 °C for 24 hours.

2.3 Synthesis of Graphene Oxide and Reduced Graphene Oxide

Graphene oxide (GO) was synthesized using the improved Hummers' method as detailed by Marcano et al. [22] and adapted in the work of Altin et al. [18]. This method involves the oxidation of graphite in a H_2SO_4/H_3PO_4 mixture with $KMnO_4$, avoiding the use of $NaNO_3$ and thus preventing the release of toxic NOx gases. The synthesized GO was then reduced to rGO. The dried GO powder was placed in a quartz beaker and subjected to microwave irradiation in a domestic microwave oven (800 W) for 120 seconds. The process resulted in a sudden, significant expansion of the GO, transforming it into a low-density, black, and fluffy powder characteristic of rGO [11, 21].

2.4 Fabrication of Composites

A hand lay-up technique was employed for composite fabrication. First, rGO powder at concentrations of 0.1, 0.2, and 0.5 wt.% relative to the epoxy resin was dispersed in the resin using an ultrasonic probe for 30 minutes to ensure uniform distribution and prevent agglomeration. The hardener was then added to the rGO/epoxy mixture at a 10:1 resin-to-hardener ratio by weight and stirred thoroughly. This mixture was then carefully applied to layers of pre-treated banana fiber mats arranged in a steel mold. A hand roller was used to facilitate complete impregnation and remove any entrapped air. A control composite with 0% rGO was also prepared. The fabricated laminates were allowed to cure at ambient temperature for 24 hours, followed by a post-curing cycle at 80 °C for 12 hours. Schematic of the fabrication process for rGO-reinforced banana fiber/epoxy composites were shown in Figure 1.

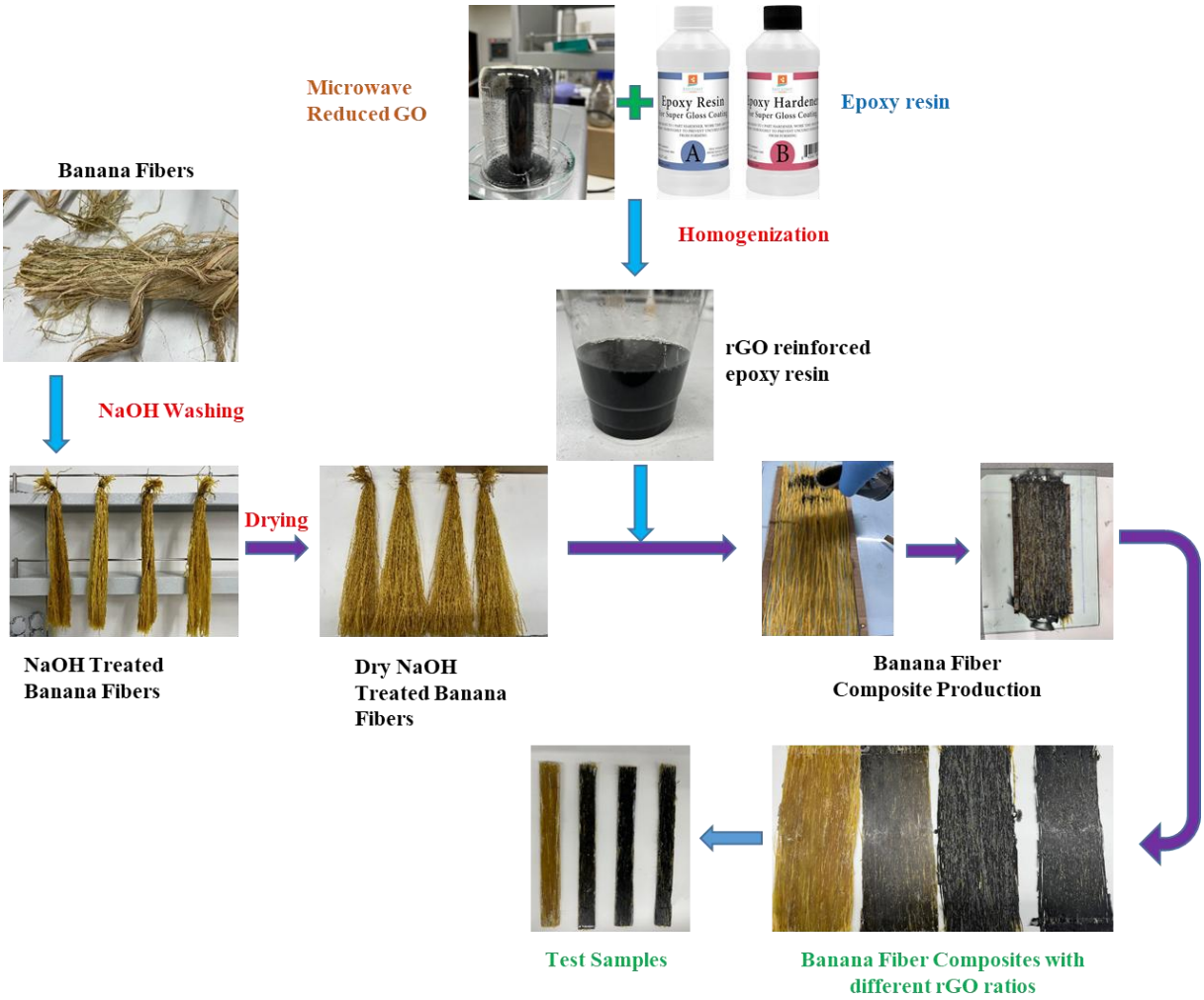

Figure 1. Schematic of the fabrication process for rGO-reinforced banana fiber/epoxy composites

2.5 Characterization

Spectroscopic Analysis: The chemical structures of the synthesized GO and rGO were characterized using Fourier-transform infrared (FT-IR) spectroscopy in the range of 4000–400 cm^{-1} with a 4 cm^{-1} spectral resolution on a Thermo scientific Nicolet i550 model FTIR spectrometer with Smart Orbit-Diamond model ATR on transmittance mode and Renishaw Invia–confocal Raman Microscope at a 532 nm laser excitation level at room temperature. FT-IR spectra were recorded to identify functional groups. Raman spectra were used to analyze the graphitic structure, disorder level (D band), and graphitic order (G band).

Mechanical Testing: Tensile tests (ASTM D3039), and three-point bending flexural tests (ASTM D790) were performed on Shimadzu-AGS-X2 universal testing machine and at least five specimens were measured for each sample and the average results were reported.

Thermal Analysis: Thermogravimetric analysis (TGA) (TA Instruments / SDT 650) was conducted to evaluate the thermal stability and char formation of the composites. Samples were heated from 30 °C to 600 °C at a heating rate of 10 °C/min under a nitrogen atmosphere to analyze the pyrolytic degradation of the organic components. Subsequently, the atmosphere was switched to oxygen, and the samples were heated from 600 °C to 900 °C at the

same rate to ensure complete oxidative combustion of the remaining carbonaceous residue. Differential scanning calorimetry (DSC) (TA Instruments / DSC250) was performed from -50 °C to 250 °C at a heating rate of 10 °C/min under a nitrogen atmosphere to determine the glass transition temperature (T_g).

Physical and Morphological Analysis: The density of the composites was measured using the Archimedes principle (ASTM D792). The fracture surfaces were examined using a Carl Zeiss / Discovery V12 Stereo Microscope.

III. RESULTS AND DISCUSSIONS

3.1 Spectroscopic Characterization

FT-IR analysis confirmed the success of each chemical modification step. The spectrum of the raw banana fiber showed a characteristic peak at ~1732 cm^{-1}, corresponding to the C=O bonds in hemicellulose and pectin (Figure 2). This peak was observed to disappear after the alkali treatment, confirming the successful removal of these amorphous, interfacial-weakening components. The final composite spectrum showed the characteristic peaks of both the banana fiber (e.g., broad O-H band at ~3359 cm^{-1}) and the cured epoxy matrix (e.g., aromatic C=C peaks at ~1606 cm^{-1} and ether C-O-C peaks at ~1236 cm^{-1}). Crucially, the disappearance of the epoxide ring peak at ~915 cm^{-1} confirmed the successful curing of the epoxy resin.

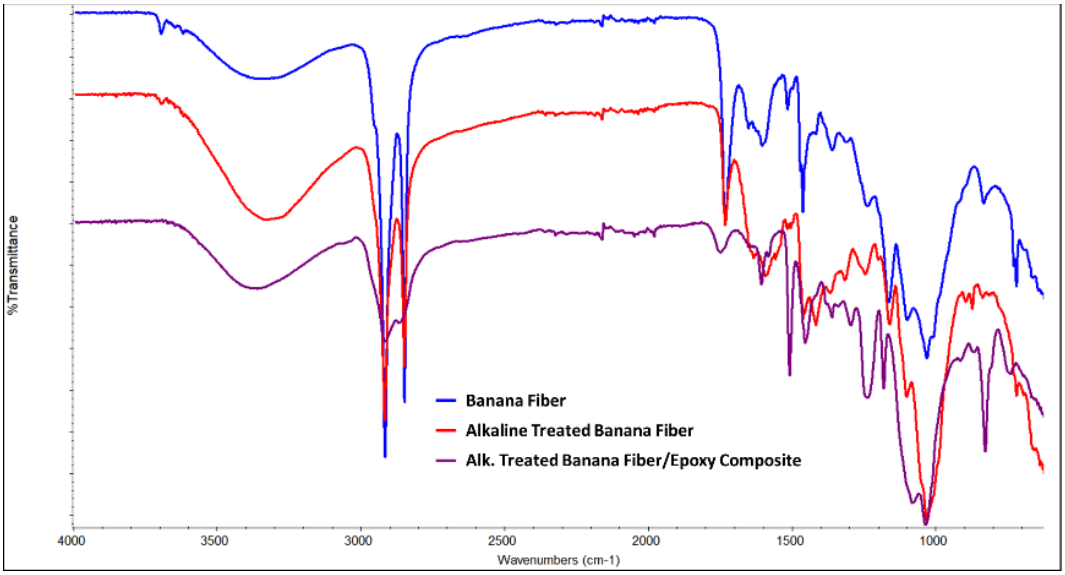

Figure 2. FT-IR spectrum of banana fiber, alkaline treated banana fiber and its composite

The FT-IR spectra of graphite, GO, and rGO are shown in Figure 3a. The spectrum of pristine graphite is a nearly flat, featureless line, which is expected for a non-polar material with no significant IR-active functional groups.

In contrast, the GO spectrum exhibits several prominent absorption peaks, confirming the successful introduction of oxygen-containing functional groups during the oxidation process. The broad and strong peak centered at 3203 cm^{-1} is attributed to the O-H stretching vibrations of hydroxyl groups and adsorbed water molecules. The sharp peak at 1715 cm^{-1} corresponds to the C=O stretching from carboxyl (-COOH) groups typically located at the edges of the GO sheets. The peak at 1621 cm^{-1} is assigned to the skeletal vibrations of the remaining unoxidized C=C

graphitic domains. Finally, the peak at 1042 cm^{-1} is characteristic of C-O stretching vibrations, likely from epoxy (C-O-C) or alkoxy groups on the basal plane [18].

After the microwave reduction process, the FT-IR spectrum of rGO shows a dramatic change. The broad O-H peak around 3200 cm^{-1} and the C=O peak at 1716 cm^{-1} are significantly diminished, indicating the effective removal of most hydroxyl and carboxyl groups. The C=C skeletal vibration peak shifts to 1557 cm^{-1}, which is closer to the G-band of pristine graphite, signifying the successful restoration of the conjugated sp^2 carbon network. The substantial reduction in the intensity of all oxygen-related peaks confirms that the microwave treatment effectively reduced the graphene oxide.

Raman spectroscopy was used to analyze the structural changes in the carbon lattice (Figure 3b). The pristine graphite spectrum shows a sharp G band (graphitic sp^2 carbon) at 1579 cm^{-1} and a very small D band (defects) at 1355 cm^{-1}. The calculated defect intensity ratio (I_D/I_G) is 0.12, indicating a highly crystalline and well-ordered graphitic structure with minimal defects.

After oxidation, the GO spectrum displays broadened D and G bands at 1341 cm^{-1} and 1586 cm^{-1}, respectively. The I_D/I_G ratio increases significantly to 0.896. This increase is a direct result of the oxidation process, which disrupts the sp^2 carbon lattice and introduces a high density of structural defects and functional groups [18, 20].

Following microwave reduction, the rGO spectrum shows a D band at 1346 cm^{-1} and a G band at 1581 cm^{-1}. Crucially, the I_D/I_G ratio increases further to 0.963. This behavior is well-documented and is a key indicator of a successful reduction process. The removal of oxygen-containing functional groups restores the electronic conjugation of the sp^2 carbon network, but it does so by creating a larger number of new, smaller graphitic domains. This increase in the density of edges and defect sites within the newly formed sp^2 clusters leads to a higher I_D/I_G ratio compared to GO [21]. While the "defect ratio" increases, the material's overall graphitic character is restored, which is essential for providing effective mechanical reinforcement in the final composite.

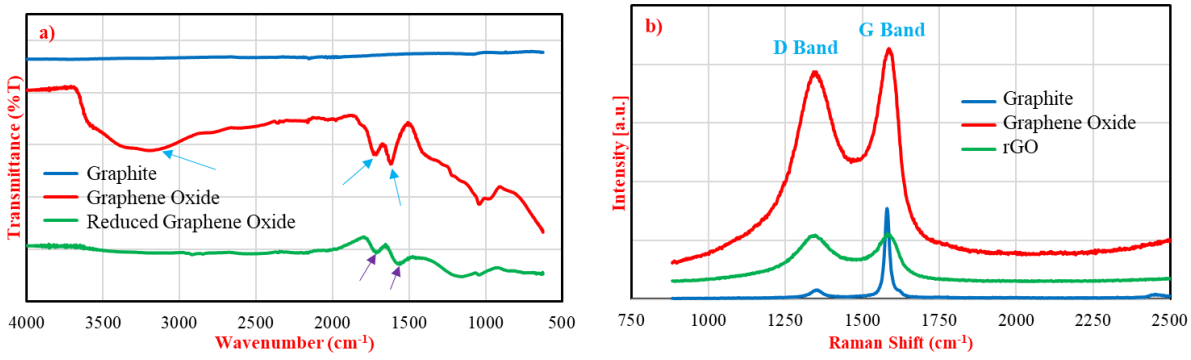

Figure 3. Spectroscopic characterization: **(a)** FT-IR spectra of Graphite, Graphene oxide, and rGO; **(b)** Raman spectra of the same materials

3.2 Mechanical Properties

3.2.1. Tensile properties

The results from the tensile tests are presented in Figure 4 and summarized in Table 1. The addition of rGO up to 0.2 wt.% led to a progressive increase in both tensile strength and tensile modulus. The neat banana fiber composite (BFC) exhibited a tensile strength of approximately 21 MPa. This value increased to 25.5 MPa for the 0.1%rGO

BFC and reached a maximum of 27 MPa for the 0.2%rGO BFC, representing a ~28% improvement over the control sample. This enhancement is attributed to the effective dispersion of rGO nanosheets at these low concentrations, which improves the interfacial adhesion between the banana fibers and the epoxy matrix, thereby facilitating more efficient stress transfer. The tensile modulus followed a similar trend, increasing from ~2000 MPa for the BFC to a peak of ~2300 MPa for the 0.2%rGO BFC, indicating an increase in stiffness.

Interestingly, a further increase in rGO content to 0.5 wt.% resulted in a significant drop in both tensile strength (~19 MPa) and modulus (~1750 MPa), with values falling below even the control sample. This sharp decline is a classic indicator of nanoparticle agglomeration. At higher concentrations, rGO sheets tend to stack together due to van der Waals forces, creating stress concentration points that act as defects and lead to premature failure under tensile load. The tensile strain values remained relatively stable across all samples, suggesting that the incorporation of rGO did not significantly alter the material's ductility at these concentrations.

The observed decrease in tensile strain beyond 0.1 wt.% rGO, despite the continued increase in strength and modulus up to 0.2 wt.%, is a characteristic behavior in reinforced polymer composites. This trend reflects a classic trade-off between stiffness and ductility. The incorporation of rigid rGO nanosheets and the resulting enhancement of interfacial adhesion create a more constrained system. This strong interface restricts the segmental mobility of the epoxy chains and hinders slippage between the fibers and the matrix under tensile load. Consequently, while the composite can withstand higher stress (increased strength), its ability to deform before fracture (ductility/strain) is reduced [23, 24].

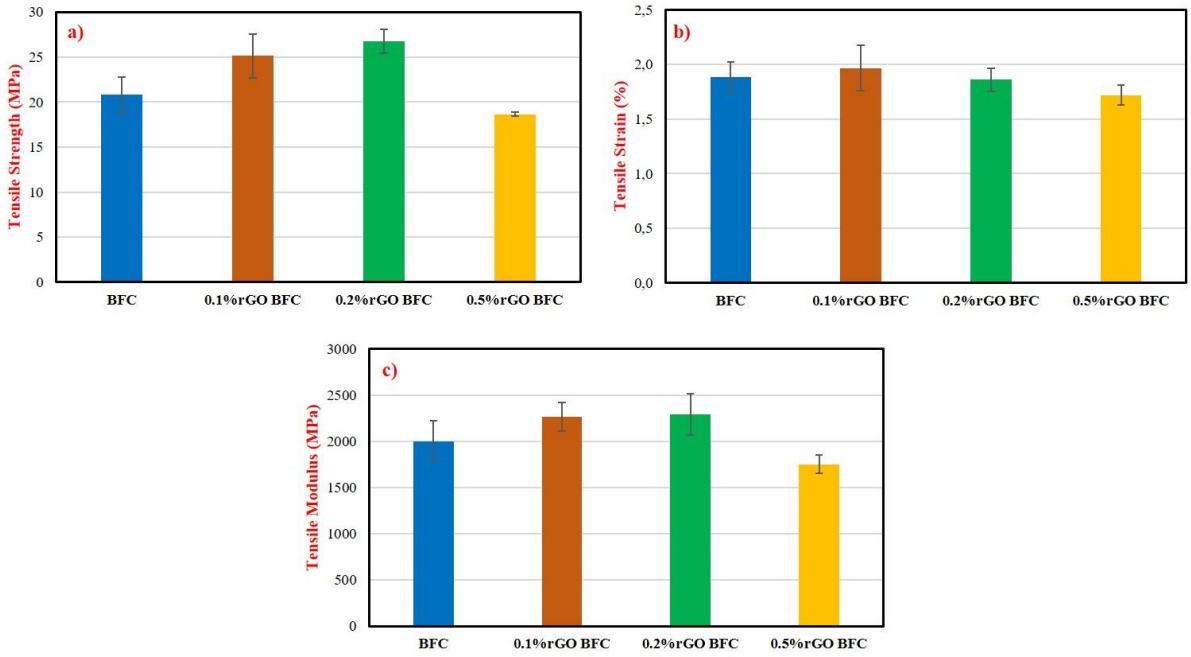

Figure 4. Tensile properties of the composites: **(a)** Tensile strength, **(b)** Tensile strain, **(c)** Tensile modulus

Table 1. Summary of tensile properties

Sample	Tensile Strength *(MPa)*	Tensile Strain *(%)*	Tensile Modulus (MPa)
BFC	20.81 ± 1.99	1.89 ± 0.14	2001 ± 219
0.1%rGO BFC	25.14 ± 2.43	1.97 ± 2.43	2264 ± 153
0.2%rGO BFC	26.75 ± 1.37	1.86 ± 0.11	2290 ± 225
0.5%rGO BFC	18.66 ± 0.25	1.72 ± 0.09	1751 ± 98

3.2.2. Flexural properties

The flexural test results, shown in Figure 5 and Table 2, presented a more complex, non-monotonic trend. The neat BFC sample had a flexural strength of ~28 MPa and a flexural modulus of ~1250 MPa. Surprisingly, the addition of 0.1% and 0.2% rGO caused a dramatic decrease in both flexural strength (to ~12 MPa and ~15 MPa, respectively) and modulus (to ~300 MPa and ~350 MPa, respectively). This non-monotonic behavior, where an initial drop in properties at very low filler loadings is followed by a significant increase, has been reported in other nanocomposite systems [25, 26].

This phenomenon can be explained by a transition in the role of the nanofiller. At very low, sub-percolating concentrations (0.1% and 0.2%), the isolated rGO nanosheets are too sparse to form a continuous, load-bearing network. Instead, they can act as stress concentration points under the complex stress state of flexural loading (combining tension, compression, and shear). These rigid, isolated platelets can disrupt the local polymer chain continuity and create micro-defects at the interface, leading to premature failure and a reduction in strength and stiffness [27]. This reduction in stiffness was accompanied by a notable increase in flexural strain, with the 0.1% rGO sample showing the highest strain value (~6.3%), indicating that the material became more deformable as its structural integrity was compromised.

In a remarkable reversal, increasing the rGO content to 0.5 wt.% resulted in a massive enhancement in performance. The 0.5%rGO BFC sample exhibited the highest flexural strength of ~49 MPa and the highest flexural modulus of ~2750 MPa. This represents a 75% increase in strength and a 120% increase in stiffness compared to the neat BFC. This behavior strongly suggests that as the concentration approaches 0.5 wt.%, the system surpasses the percolation threshold. At this point, the rGO sheets begin to form an effective, interconnected reinforcing network throughout the matrix. This network provides a significant stiffening effect and efficiently resists bending forces, leading to the observed dramatic increase in both strength and modulus [28]. The significant increase in stiffness at this concentration is mirrored by a sharp decrease in flexural strain (to ~2.8%), indicating that the composite became much more rigid and brittle, a typical trade-off for high-strength composites. This highlights that the optimal rGO concentration is highly dependent on the type of mechanical loading.

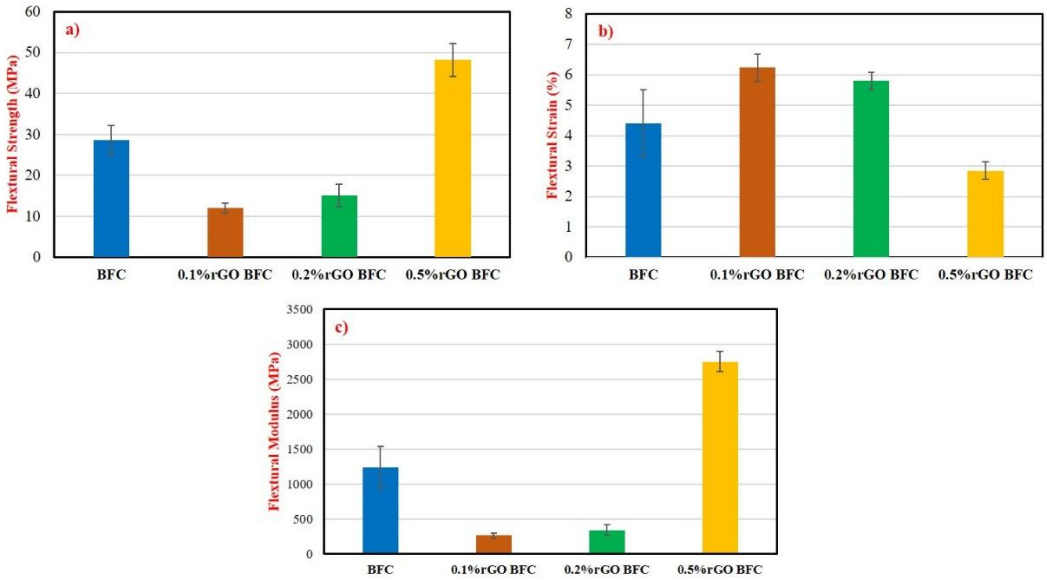

Figure 5. Flexural properties of the composites: **(a)** Flexural Strength, **(b)** Flexural Strain, **(c)** Flexural Modulus

Table 2. Summary of flexural properties

Sample	Flexural Strength *(MPa)*	Flexural Strain *(%)*	Flexural Modulus (MPa)
BFC	28.56 ± 3.59	4.40 ± 1.11	1233 ± 307
0.1%rGO BFC	12.05 ± 1.20	6.23 ± 0.46	264 ± 36
0.2%rGO BFC	15.16 ± 2.74	5.80 ± 0.29	342 ± 74
0.5%rGO BFC	48.18 ± 3.99	2.85 ± 0.29	2752 ± 146

3.3 Thermal Properties

The thermal behavior of the fabricated composites was investigated using TGA and DSC to understand the effect of rGO on their thermal stability and polymer chain dynamics.

3.3.1. Thermogravimetric analysis (TGA)

The TGA curves, which show the weight loss of the composites as a function of temperature, are presented in Figure 6. The primary weight loss event for all composites occurs between 250 °C and 450 °C under the inert nitrogen atmosphere. To provide a clearer and more precise comparison of thermal stability, the inset graph in Figure 6 focuses on the initial degradation region, specifically showing the temperature at which each sample reaches 75% of its initial weight (i.e., 25% degradation). The exact temperatures for this 25% weight loss ($T_{d25\%}$) are summarized in Table 3.

The data reveals a clear trend of enhanced thermal stability with rGO addition. The $T_{d25\%}$ temperature increases from 307.7 °C for the neat BFC to 318.0 °C for 0.1% rGO, reaching a maximum of 322.9 °C for the composite containing 0.2 wt.% rGO. This represents a significant increase of over 15 °C, quantitatively confirming a substantial improvement in thermal stability. This enhancement is attributed to the "barrier effect" of the well-dispersed rGO nanosheets. These impermeable sheets create a tortuous path that hinders heat transfer and slows the diffusion of volatile degradation products, thus delaying decomposition [20, 29].

The slight decrease in stability for the 0.5% rGO sample ($T_{d25\%}$= 319.2 °C) compared to the 0.2% sample aligns with the mechanical property data and is likely due to the onset of rGO agglomeration, which reduces the homogeneity and effectiveness of the barrier network.

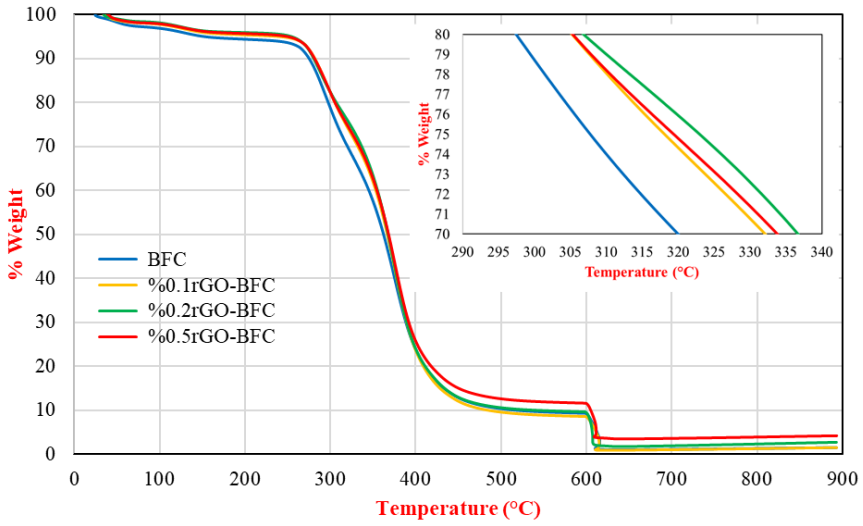

Figure 6. TGA thermograms of BFC and rGO-BFC composites. The inset shows a magnified view of the degradation, focusing on the temperature at which 75% weight remains

3.3.2. Differential scanning calorimetry (DSC)

The DSC analysis provided profound insights into the polymer-nanofiller interactions, as shown in Figure 7 and summarized in Table 3. The DSC curve for the neat BFC sample showed a single, clear glass transition temperature (T_g) at 112.21 °C, representing the bulk epoxy matrix.

Remarkably, the addition of rGO led to the appearance of two distinct glass transition temperatures in all modified composites. This phenomenon is characteristic of nanocomposites with strong interfacial interactions, indicating the formation of two different regions with distinct polymer chain mobilities:

1. Bulk Matrix Phase (T_{g1}): The first T_g, observed in the 131-132 °C range, corresponds to the bulk epoxy matrix which is relatively far from the rGO nanofillers. The T_{g1} for all rGO-filled samples is significantly higher than that of the neat BFC. It increased from 112.21 °C to a maximum of 132.23 °C for the 0.2% rGO sample. This indicates that even the bulk matrix benefits from a long-range stiffening effect imparted by the dispersed rGO network.
2. Constrained Interphase Region (T_{g2}): A second, new T_g appears at a much higher temperature, around ~160 °C, for all rGO-containing samples. This higher T_g is attributed to the formation of a "rigid amorphous fraction" or a constrained polymer interphase immediately surrounding the rGO nanosheets. The large surface area of rGO creates strong physical and chemical interactions with the adjacent epoxy chains, severely restricting their segmental mobility. Consequently, a much higher thermal energy is required to induce glass transition in this region [1, 30].

The presence of this high-temperature T_{g2} is direct and powerful evidence of effective reinforcement and strong interfacial adhesion created by the rGO. The fact that the bulk Tg_1 also peaks at 0.2 wt.% rGO further supports the conclusion that this concentration provides the most optimized and homogeneous dispersion, leading to the best overall improvement in the matrix's structural integrity.

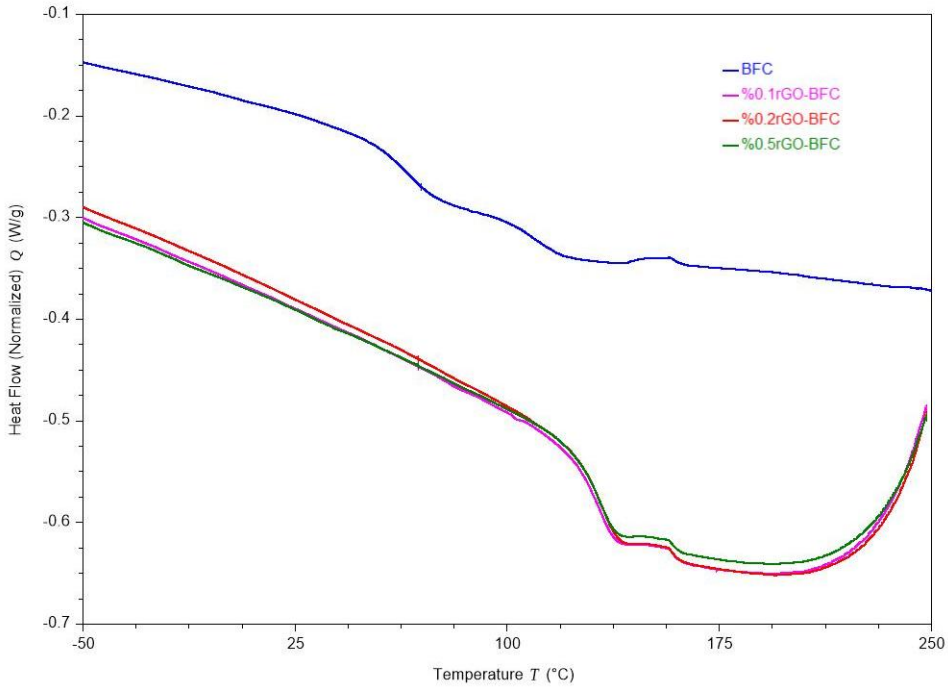

Figure 7. DSC curves for BFC and rGO-BFC composites, showing the presence of multiple glass transitions

Table 3. Summary of Thermal Properties from TGA and DSC

Sample	$T_{d25\%}$ (°C) from TGA (in N_2)	Bulk T_{g1} (°C)	Interphase T_{g2} (°C)
BFC	307.7	112.21	160.2
0.1%rGO BFC	318.0	131.44	160.1
0.2%rGO BFC	322.9	132.23	159.0
0.5%rGO BFC	319.2	131.14	159.3

3.4 Physical and Morphological Properties

The physical properties, specifically the fiber content and density, of the fabricated composites were analyzed to understand their microstructural integrity. The results are presented in Figure 8.

As shown in Figure 8a, the calculated final fiber content in the composites shows an increasing trend with the addition of rGO, rising from approximately 9.2% for the neat BFC to 13.8% for the 0.5%rGO BFC sample. This reflects the formulation where rGO was added to the matrix, slightly altering the relative weight fractions of the constituents.

Conversely, the experimental density measurements, shown in Figure 8b, reveal a significant and generally decreasing trend with increasing reinforcement content. The neat BFC sample exhibited the highest density at approximately 1.08 g/cm³. The density then decreased for the rGO-containing samples, reaching a minimum of 0.98 g/cm³ for the 0.5%rGO BFC composite.

This inverse relationship between the increasing reinforcement content (fiber + rGO) and the decreasing overall composite density can be directly attributed to the inherent porosity of the natural banana fibers. Microscopic examination reveals that banana fibers possess a hollow internal structure known as a lumen [7, 10]. As the volume fraction of these fibers increases in the composite, the volume fraction of these intrinsic voids also increases. These voids, if not perfectly filled by the epoxy resin during fabrication, contribute to a lower overall density. The lowest density observed in the 0.5%rGO BFC sample, which has the highest fiber content, strongly supports this conclusion. While rGO itself is dense, its contribution to the overall volume is minimal; the dominant effect on density in this system comes from the porous nature of the banana fiber reinforcement. This finding is crucial for the design of lightweight composites, as it indicates that higher fiber loading does not linearly translate to higher weight, but it also highlights the challenge of void formation.

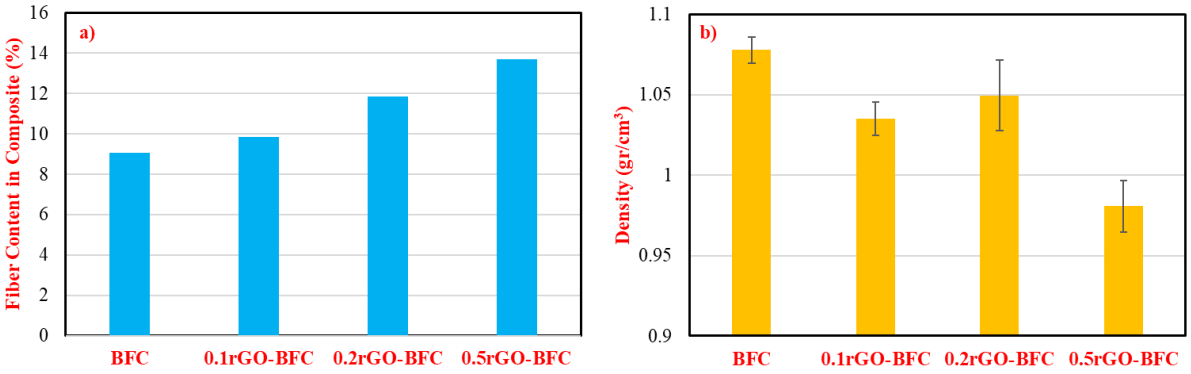

Figure 8. Physical properties of the composites: **(a)** Calculated final fiber content and **(b)** Experimental density

Optical microscopy was used to examine the cross-sectional morphology of the composites (Figure 9). Figure 9a, showing the composite with 0.2 wt.% rGO, reveals a generally homogeneous distribution of the banana fibers

within the dark epoxy matrix. However, some visible voids, highlighted in the image, are also present. These voids are consistent with the lumen structure of the fibers and the challenges of achieving perfect impregnation with the hand lay-up technique.

Similarly, the micrograph of the composite with 0.5 wt.% rGO (Figure 9b) also displays a uniform distribution of reinforcement. The effective and homogeneous dispersion of both the fibers and the rGO nanofiller throughout the matrix is a critical prerequisite for achieving good mechanical properties, as it ensures that stress can be transferred and distributed evenly within the material. While the density data suggests a higher overall void content in the 0.5% rGO sample, its superior flexural performance indicates that the formation of a well-distributed and interconnected reinforcing network at this concentration is the dominant factor for resisting bending loads. This network's ability to withstand flexural stress outweighs the negative impact of the increased porosity. This observation supports the conclusion that different rGO concentrations trigger different dominant reinforcing mechanisms depending on the type of mechanical stress applied.

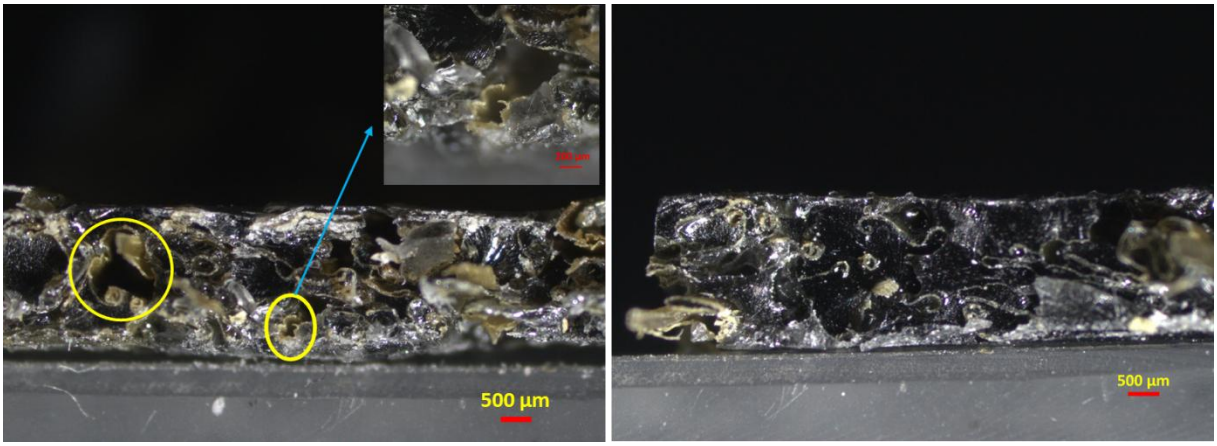

Figure 9. Optical micrographs of the cross-section of (a) 0.2%rGO BFC, showing fiber lumens and voids (inset shows a magnified view), and (b) 0.5%rGO BFC, showing a more compact structure

IV. CONCLUSIONS

This study successfully demonstrated the fabrication and characterization of banana fiber-reinforced epoxy composites enhanced with microwave-reduced graphene oxide. The key conclusions are:

1. FT-IR and Raman spectroscopy analyses successfully confirmed the oxidation of graphite to GO and its subsequent, effective reduction to rGO.
2. The effect of rGO on the mechanical properties of banana fiber composites is complex, with tensile properties optimized at 0.2 wt.% rGO and flexural properties at 0.5 wt.%.
3. TGA and DSC results confirmed that rGO addition improved the thermal stability of the composites.
4. Physical and morphological analyses revealed that the composite's density is strongly influenced by the inherent porosity (lumen) of the banana fibers. Optical microscopy confirmed the homogeneous distribution of the fibers, which is essential for load transfer, while also highlighting the presence of process- and fiber-related voids that contribute to the lower density at higher reinforcement loadings.

5. These findings underscore that there is no single "optimal" nanofiller concentration; it must be tailored to the specific application, considering the trade-offs between mechanical, thermal, and physical properties.

This research demonstrates that microwave-assisted synthesis is a viable route for producing rGO, and its incorporation at an optimal level can effectively enhance the performance of natural fiber composites, paving the way for their use in more demanding structural applications.

ACKNOWLEDGMENT

The authors would like to extend their special thanks to Dr. Sibel Tuna and Zeynep Aksoy for their valuable assistance in performing the Raman spectroscopy analysis.

REFERENCES

1. Luz FSD, Garcia Filho FDC, Gómez del-Río MT et al (2020) Graphene-incorporated natural fiber polymer composites: a first overview. Polymers 12(7):1601. https://doi.org/10.3390/polym12071601
2. Sanjay MR, Madhu P, Jawaid M et al (2018) Characterization and properties of natural fiber polymer composites: A comprehensive review. Journal of Cleaner Production 172:566-581. https://doi.org/10.1016/j.jclepro.2017.10.101
3. Pickering, KL, Efendy, MA, Le, TM (2016) A review of recent developments in natural fibre composites and their mechanical performance. Composites Part A: Applied Science and Manufacturing 83:98-112. https://doi.org/10.1016/j.compositesa.2015.08.038
4. Verma G, Goel R, Kaur N et al (2025) Understanding behaviour of graphene in natural fibre composites: a comprehensive review. European Polymer Journal 232:113959. https://doi.org/10.1016/j.eurpolymj.2025.113959
5. Peças P, Carvalho H, Salman H, Leite M (2018) Natural Fibre Composites and Their Applications: A Review. Journal of Composites Science 2(4):66. https://doi.org/10.3390/jcs2040066
6. Sapuan SM, Leenie A, Harimi M, Beng YK (2006) Mechanical properties of woven banana fibre reinforced epoxy composites. Materials and Design 27(8):689-693. https://doi.org/10.1016/j.matdes.2005.03.028
7. Assis FS, Monteiro SN, Margem FM, Loiola RL (2014) Charpy toughness behavior of continuous banana fiber reinforced epoxy matrix composites. In: Carpenter J S et al (ed) Characterization of minerals, metals, and materials, Springer, Cham, (pp. 499-506). https://doi.org/10.1002/9781118888056.ch58
8. Kumar SCR, Shivanand HK, Vidayasagar HN, Nagabhushan V (2018) Studies on mechanical properties of graphene based hybrid composites reinforced with kenaf/glass fiber. AIP Conference Proceedings 1943:020115. https://doi.org/10.1063/1.5050735
9. Papageorgiou DG, Kinloch IA, Young RJ (2017) Mechanical properties of graphene and graphene-based nanocomposites. Progress in Materials Science, 90:75-127. https://doi.org/10.1016/j.pmatsci.2017.02.003
10. Arunkumar K, Murugarajan A (2022) Investigation of mechanical properties and free vibration behavior of graphene/basalt nano filler banana/sisal hybrid composite. Polymers and Polymer Composites 30. https://doi.org/10.1177/09673911211066719
11. Bharadiya PS, Singh MK, Mishra S (2019) Influence of graphene oxide on mechanical and hydrophilic properties of epoxy/banana fiber composites. JOM 71(2):838–843. https://doi.org/10.1007/s11837-018-3239-8
12. Görür M, Özel Ş, Olgun A, Tiritoğlu M (2024) An adhesive composite material from magnetite and a methacrylate copolymer with epoxy and PEG side groups. ChemistrySelect 9(48):e202402390. https://doi.org/10.1002/slct.202402390
13. Gupta US, Tiwari S, Sharma U (2023) Influence of low-pressure Ar plasma modification of Musa sapientum banana fibers on banana fiber reinforced epoxy composite. Composite Interfaces 30(8):877-898. https://doi.org/10.1080/09243046.2019.1709679
14. Kaliyaperumal G, Nedunchezhiyan M, Natesan P et al (2023) Recycle of bio-waste banana and sisal fiber filled harmlessness epoxy hybrid composite for automotive roof application. Environmental Quality Management 33(1):165-171. https://doi.org/10.1002/tqem.22039

15. Özen S, Benlioğlu A, Mardani A, Altın Y, Bedeloğlu A (2024) Effect of graphene oxide-coated jute fiber on mechanical and durability properties of concrete mixtures. Construction and Building Materials 448:138225. https://doi.org/10.1016/j.conbuildmat.2024.138225
16. Novoselov KS, Geim AK, Morozov SV, Jiang, D et al (2004) Electric field effect in atomically thin carbon films. Science 306(5696):666-669. https://doi.org/10.1126/science.1102896
17. Stankovich S, Dikin DA, Piner RD et al (2007) Synthesis of graphene-based nanosheets via chemical reduction of exfoliated graphite oxide. Carbon 45(7):1558-1565. https://doi.org/10.1016/j.carbon.2007.02.034
18. Altin Y, Yilmaz H, Unsal OF, Bedeloglu AC (2020) Graphene oxide modified carbon fiber reinforced epoxy composites. Journal of Polymer Engineering 40(5):415-420. https://doi.org/10.1515/polyeng-2020-0033
19. Bharadiya PS, Puri RG, Mishra S (2024) Enriched mechanical properties of graphite nanoplatelets filled epoxy resin-plant fiber nanocomposites. Polymer Bulletin 81:4275–4289. https://doi.org/10.1007/s00289-023-04938-z
20. Jakhar R, Yap JE, Joshi R (2020) Microwave reduction of graphene oxide. Carbon 170:277-293. https://doi.org/10.1016/j.carbon.2020.01.056
21. Xie X, Zhou Y, Huang K (2019) Advances in microwave-assisted production of reduced graphene oxide. Frontiers in Chemistry 7:355. https://doi.org/10.3389/fchem.2019.00355
22. Marcano DC, Kosynkin DV, Berlin JM et al (2010) Improved synthesis of graphene oxide. ACS Nano 4(8):4806-4814. https://doi.org/10.1021/nn1006368
23. Ikramullah Rizal S, Nakai Y, Shiozawa D, Khalil HA, Huzni S, Thalib S (2019) Evaluation of interfacial fracture toughness and interfacial shear strength of Typha spp. fiber/polymer composite by double shear test method. Materials 12(14):2225. https://doi.org/10.3390/ma12142225
24. Abu Bakar AA, Zainuddin MZ, Abdullah SM, Tamchek N et al (2022) The 3D printability and mechanical properties of polyhydroxybutyrate (PHB) as additives in urethane dimethacrylate (UDMA) blends polymer for medical application. Polymers 14(21):4518. https://doi.org/10.3390/polym14214518
25. Joshi R, Bajpai PK, Mukhopadhyay S (2023) Processing and performance evaluation of agro wastes reinforced bio-based epoxy hybrid composites. Proceedings of the Institution of Mechanical Engineers, Part L: Journal of Materials: Design and Applications 237(2):482-499. https://doi.org/10.1177/09544062221125105
26. Aminullah A, Syed Mustafa SJ, Nor Azlan MR, Mohd Hafizi N, Mohd Ishak ZA, Rozman HD (2010) Effect of filler composition and incorporation of additives on the mechanical properties of polypropylene composites with high loading lignocellulosic materials. Journal of Reinforced Plastics and Composites 29(20):3115-3124. https://doi.org/10.1177/0731684410381490
27. Dobrosielska M, Dobrucka R, Kozera P, Brząkalski D et al (2023) Beeswax as a natural alternative to synthetic waxes for fabrication of PLA/diatomaceous earth composites. Scientific Reports 13(1):1161. https://doi.org/10.1038/s41598-023-29708-5
28. Fronza BM, Ayres APA, Pacheco RR, Rueggeberg FA, Dias CTDS, Giannini M (2017) Characterization of inorganic filler content, mechanical properties, and light transmission of bulk-fill resin composites. Operative Dentistry 42(4):445-455. https://doi.org/10.2344/oper-16-113
29. Rath SK, Prusty RK (2021) Review on thermal stability and fire-retardant properties of natural fiber-reinforced polymer composites. Polymer Composites 42(4):1547-1572. https://doi.org/10.1002/pc.32800
30. Papageorgiou DG, Kinloch IA, Young RJ (2017) Mechanical properties of graphene and graphene-based nanocomposites. Progress in Materials Science 90:75-127. https://doi.org/10.1016/j.pmatsci.2017.02.003